In Situ Analysis of Opal in Gale Crater, Mars

Rapin, W.; Chauviré, B.; Gabriel, T. S. J.; Mcadam, A. C.; Ehlmann, B. L.; Hardgrove, C.; Meslin, P.-y.; Rondeau, B.; Dehouck, E.; Franz, H. B.; Mangold, N.; Chipera, S. J.; Wiens, R. C.; Frydenvang, J.; Schröder, S.

Published in:
Journal of Geophysical Research: Planets

DOI:
10.1029/2017JE005483

Publication date:
2018

Document version
Publisher's PDF, also known as Version of record

Journal of Geophysical Research: Planets

RESEARCH ARTICLE
10.1029/2017JE005483

Key Points:
- Sedimentary rocks with high amorphous silica content were analyzed at Gale crater on Mars
- Calibration of the LIBS hydrogen signal reveals >4 wt% water content associated with silica
- The stability of opal-A over several billion years is an anomaly relative to terrestrial mineralogy

Supporting Information:
- Supporting Information S1
- Data S1
- Data S2

Correspondence to:
W. Rapin,
wrapin@caltech.edu

Citation:
Rapin, W., Chauviré, B., Gabriel, T. S. J., McAdam, A. C., Ehlmann, B. L., Hardgrove, C., et al. (2018). In situ analysis of opal in Gale crater, Mars. *Journal of Geophysical Research: Planets*, *123*, 1955–1972. https://doi.org/10.1029/2017JE005483

Received 9 NOV 2017
Accepted 12 JUN 2018
Accepted article online 3 JUL 2018
Published online 4 AUG 2018

The copyright line for this article was changed on 20 AUG 2018 after original online publication.

In Situ Analysis of Opal in Gale Crater, Mars

W. Rapin[1], B. Chauviré[2,3], T. S. J. Gabriel[4], A. C. McAdam[5], B. L. Ehlmann[1,6], C. Hardgrove[4], P.-Y. Meslin[7], B. Rondeau[8], E. Dehouck[7,9], H. B. Franz[5], N. Mangold[8], S. J. Chipera[10], R. C. Wiens[11], J. Frydenvang[12], and S. Schröder[7,13]

[1]Division of Geological and Planetary Sciences, California Institute of Technology, Pasadena, CA, USA, [2]School of Mathematical and Physical Sciences, University of Technology, Sydney, New South Wales, Australia, [3]Dr. Eduard Gübelin Association for Research and Identification of Precious Stones, Lucerne, Switzerland, [4]School of Earth and Space Exploration, Arizona State University, Tempe, AZ, USA, [5]NASA Goddard Space Flight Center, Greenbelt, MD, USA, [6]Jet Propulsion Laboratory, California Institute of Technology, Pasadena, CA, USA, [7]Institut de Recherche en Astrophysique et Planétologie, Université de Toulouse, CNRS, UPS, CNES, Toulouse, France, [8]Laboratoire de Planétologie et Géodynamique, Université de Nantes, Nantes, France, [9]Université de Lyon, UCBL, ENSL, CNRS, LGL-TPE, Villeurbanne, France, [10]Chesapeake Energy, Oklahoma City, OK, USA, [11]Los Alamos National Laboratory, Los Alamos, NM, USA, [12]Natural History Museum of Denmark, University of Copenhagen, Copenhagen, Denmark, [13]German Aerospace Center (DLR), Institut für Optische Sensorsysteme, Berlin-Adlershof, Germany

Abstract Silica enrichments resulting in up to ~90 wt% SiO_2 have been observed by the Curiosity rover's instruments in Gale crater, Mars, within the Murray and Stimson formations. Samples acquired by the rover drill revealed a significant abundance of an X-ray amorphous silica phase. Laser-induced breakdown spectroscopy (LIBS) highlights an overall correlation of the hydrogen signal with silica content for these Si-enriched targets. The increased hydration of the high-silica rocks compared to the surrounding bedrock is also confirmed by active neutron spectroscopy. Laboratory LIBS experiments have been performed to calibrate the hydrogen signal and show that the correlation observed on Mars is consistent with a silica phase containing on average 6.3 ± 1.4 wt% water. X-ray diffraction and LIBS measurements indicate that opal-A, amorphous hydrated silica, is the most likely phase containing this water in the rocks. Pyrolysis experiments were also performed on drilled samples by the Sample Analysis at Mars (SAM) instrument to measure volatile content, but the data suggests that most of the water was released during handling prior to pyrolysis. The inferred low-temperature release of water helps constrain the nature of the opal. Given the geological context and the spatial association with other phases such as calcium sulfates, the opal was likely formed from multiple diagenetic fluid events and possibly represents the latest significant water-rock interaction in these sedimentary rocks.

1. Introduction

Opal is a hydrated amorphous to poorly crystalline variety of silica, which mostly precipitates from liquid water. On Earth, it is found in various geological environments, for instance, in hydrothermal settings (Jones & Renaut, 2004; Lynne et al., 2005; Rodgers et al., 2004), within continental weathering profiles (Chauviré, Rondeau, Mazzero, et al., 2017; Rondeau et al., 2012; Thiry & Milnes, 1991; Thiry et al., 2006), or in marine sediments (Behl, 2011; Meister et al., 2014; Murata & Nakata, 1974). Although many processes produce opal on Earth due to the abundance of silica and liquid water at the surface, diagenesis typically transforms opal into quartz, a more stable form of silica (Williams & Crerar, 1985; Williams et al., 1985). Mars' surface is mostly dominated by a basaltic composition, but given the mobility of silica from basalt under most weathering conditions and the evidence for liquid water in Mars' past, significant amounts of sedimentary silica could have formed (McLennan, 2003).

The distinction between the various forms of hydrated silica is important due to the contrasting implications for their geologic origin. The main categories can be ordered by increasing degree of crystallinity: hydrated glasses, opals, and microcrystalline quartz (Flörke et al., 1991). Hydrated silicate glasses form directly by quenching of hydrous melts. They are structurally amorphous, or poorly crystalline, and retain small amounts of H_2O and OH, isolated and structurally bound (Stolper, 1982). The microstructure of opal is characterized by an assemblage of silica nanograins that can retain water (H_2O), either adsorbed or trapped in voids, as well as hydroxyl groups in silanols (Si-OH; Anderson & Wickersheim, 1964; Boboň et al., 2011; Gaillou et al., 2008;

Langer & Flörke, 1974). Opals precipitate from solution and mostly exist as opal-A (amorphous) and opal-CT, which has nanodomains of cristobalite (C) with some tridymite (T) stacking and may be organized in microspherules or lepispheres. Compared to silica glasses, the porosity of opals enables more molecular water to be present (up to 10 wt%; e.g., Flörke et al., 1991; Graetsch et al., 1994; Thomas et al., 2010), trapped in voids or forming interstitial films (Langer & Flörke, 1974; Segnit et al., 1965). Opals are metastable at the Earth's surface temperatures and pressures and usually evolve by dissolution and reprecipitation following the pathway: opal-A → opal-CT → microcrystalline quartz (Williams & Crerar, 1985). Indeed, chalcedony or other types of microcrystalline quartz may result from the diagenesis of opals but can also precipitate directly from solution under specific conditions (Graetsch et al., 1985). Microcrystalline quartz typically has lower porosity and therefore contains less water than opals, rarely more than 2 wt% for molecular water and hydroxyl groups combined (Flörke et al., 1982, 1991; Schmidt & Fröhlich, 2011).

The bonding of water molecules and hydroxyl groups in opals creates a variety of spectral features that can be used for identification on Mars by near-infrared remote sensing (Chauviré, Rondeau, & Mangold, 2017; Goryniuk et al., 2004). In particular, opals are characterized by absorption bands at 2.21–2.26 μm due to silanols combined with those attributed to molecular water (free or hydrogen-bounded to silanols) at 1.91–1.96 μm (Boboň et al., 2011). However, silica varieties other than opal, like silica glasses, or microcrystalline quartz, can also contain silanols and adsorbed water. Although these can produce subtle changes in the absorption band shape, depth, and position, such differences usually remain challenging to identify in practice (Milliken et al., 2008; Rice et al., 2013; Smith et al., 2013). Therefore, "hydrated silica" or "opaline silica" have been reported on the Martian surface depending on the level of confidence that the observed spectra are similar to those from opals observed in the laboratory.

Hydrated silica was identified in a variety of terrains on Mars from the Noachian and Hesperian eras. Using the CRISM (Compact Reconnaissance Imaging Spectrometer for Mars) instrument, opaline silica was reported in strata on plains surrounding Valles Marineris, associated with sulfates, and interpreted as a direct precipitate that formed a silica cement or altered volcanic material (Milliken et al., 2008; Weitz et al., 2010). It was also observed in layers near fan deposits inside the canyon system (Metz et al., 2009). Hydrated silica was identified in deposits of likely hydrothermal origin on the flanks of a volcanic cone in Syrtis Major (Skok et al., 2010). It was also found associated with phyllosilicates in Terra Sirenum possibly related to alteration by groundwater (Wray et al., 2011) and in Nili Fossae in the form of eolian deposits, associated with material eroded from crater central peaks (Ehlmann et al., 2009). In a more global impact craters survey, it is detected within a number of eolian/unconsolidated deposits (Sun & Milliken, 2015). In addition, extensive areas in western Hellas show evidence for hydrated silica, probably due to late stage alteration with groundwater (Bandfield et al., 2013). These examples of hydrated silica detections from orbit highlight the diverse settings in which opals may be found on Mars.

In situ, the Opportunity rover identified up to 25 wt% hydrated silica along with phyllosilicates in an outcrop at Meridiani Planum, according to the modeling of thermal infrared spectra from the Mini-TES instrument (Glotch et al., 2006). Spirit observed high silica in Gusev Crater near "Home Plate," a formation interpreted as volcanoclastic, within light-toned nodular bedrock and soils (Ruff et al., 2011). The content of silica measured there by Spirit's APXS (Alpha Particle X-Ray Spectrometer) reached up to 92 wt% (H-free normalization) in the light-toned soils, and the most likely silica phase is opal according to thermal infrared emission spectra (Mini-TES), which include absorption bands due to molecular water at 1,630/cm and silanols near 900/cm. However, limitations inherent to the rover instrument suite prevented further characterization of the silica, including opal type and water content.

At Gale crater, the Curiosity rover landed with new instruments dedicated to geochemistry and mineralogy. On its traverse toward the lower slopes of Mt Sharp, the rover explored a sequence of fluvial, deltaic, and lacustrine sedimentary rocks (Grotzinger et al., 2015). Weak signatures of hydrated silica were identified from orbit using CRISM data in some patches within the sedimentary rocks of Mt. Sharp but were not directly on the path taken by the rover (Fraeman et al., 2016; Seelos et al., 2014). Yet silica enrichments were observed in situ by the rover in an outcrop of finely laminated mudstone within the Murray formation: a drill sample collected in the mudstone and analyzed by CheMin, the X-ray diffraction instrument, revealed ~14 wt% tridymite, of likely detrital origin, along with ~60 wt% of silica-rich amorphous phases (Morris et al., 2016). High silica abundance was also measured within fracture-associated alteration halos present in the mudstone and across the unconformably overlying eolian sandstone in the Stimson formation (Frydenvang et al.,

2017; Yen et al., 2017). Drill samples from these alteration halos also show the presence of a significant silica-rich amorphous component compared to the surrounding unaltered bedrock (Yen et al., 2017).

X-ray diffraction measurements alone cannot distinguish between opal-A and glasses. Both fit in the broad background signal that is visible in the diffraction pattern of the high-silica drill samples (Morris et al., 2016; Yen et al., 2017). In addition to CheMin, the silica-rich rocks were analyzed by other instruments sensitive to hydration. The SAM (Sample Analysis at Mars) instrument (Mahaffy et al., 2012) performed pyrolysis and evolved gas analyses (EGAs) of the same drill samples and measured the release of water molecules with temperature (Sutter et al., 2017). Furthermore, the DAN (Dynamic Albedo of Neutron) instrument measured the abundance of water in the shallow subsurface (up to ~60 cm) since variations in hydrogen content can result in detectable changes in their data due to the large scattering cross section of hydrogen with neutrons (Mitrofanov et al., 2012). Finally, the ChemCam instrument used laser-induced breakdown spectroscopy (LIBS) to measure the abundance of major, minor, and trace elements at a submillimeter scale (Maurice et al., 2016; Wiens et al., 2015). Using this technique ChemCam directly detects hydrogen and can be used to quantify water content in a variety of geological materials (Rapin et al., 2017a).

The objective of this study is to investigate the characteristics of the silica phase observed at Gale crater. In contrast with previous studies (Frydenvang et al., 2017; Morris et al., 2016; Yen et al., 2017), we focus on the amorphous silica phase and combine data from the ChemCam instrument with DAN and SAM to assess its nature. We first focus on ChemCam data and determine the specific calibration of the hydrogen signal with opals using the instrument's laboratory replica. Then the results are applied to the Mars data set and compared with data from the other instruments.

2. Materials and Methods

2.1. Instrument Description

The ChemCam instrument provides elemental compositions of remote targets (up to 7 m away) at a submillimeter scale using LIBS (Maurice et al., 2012; Wiens et al., 2012). Hydrogen is detected by the Balmer alpha emission peak at 656.5 nm; other hydrogen peaks lie outside of the spectrometer range. Typical ChemCam observations consist of bursts of 30 laser shots on a given point, which is repeated on several points at closely spaced distances from one another on the target. Due to the surface ablation by the laser and the plasma shockwave, dust is effectively removed by the first shots, enabling measurement of the substrate without influence from surface-deposited materials. This dust-removal ability is particularly important for studying the hydrogen content of the rock substrate because the dust that coats rocks on Mars is known to be hydrated (e.g., Meslin et al., 2013; Audouard et al., 2014). ChemCam also provides high-resolution images, which help identify the analyzed locations and document the surface texture of the targets.

The laboratory LIBS setup at Institut de Recherche en Astrophysique et Planétologie (IRAP, Toulouse, France) uses the ChemCam instrument replica as described in Rapin et al. (2017a). Targets are located at a distance of 1.7 m from the instrument in a vacuum chamber whose pressure can be lowered to below 10^{-3} mbar before introducing a Martian atmospheric gas simulant (1.6% argon, 2.7% nitrogen, and 95.7% carbon dioxide) to produce LIBS plasmas in conditions similar to Mars, under ~8 mbar atmospheric pressure.

2.2. Opal Sample Preparation

A series of natural opals and a chalcedony, part of a collection described in Chauviré, Rondeau, and Mangold (2017), were analyzed for the calibration of the LIBS hydrogen signal. Each opal sample was characterized by Raman spectroscopy to determine the opal type (opal-A or opal-CT) and transmission infrared spectroscopy to estimate homogeneity of molecular water and silanol (hydroxyl group; Si-OH) contents (Chauviré, Rondeau, & Mangold, 2017). Homogeneous bulk fragments with sizes between 3 and 5 mm were selected for analysis using the ChemCam laboratory LIBS setup.

Opal samples are known to lose a potentially significant amount of water when exposed to vacuum (Segnit et al., 1965). As shown in a previous study where water vapor was added to the Martian gas simulant (Rapin et al., 2017a), a hydrogen LIBS signal due to the atmosphere is observed at $\geq$0.1 mbar of water vapor partial pressure. Such an amount could be produced from degassing of opals at low pressure; therefore, the samples were first placed under dynamic vacuum for 20 hr. Then, after introducing the Martian

Table 1
Characteristics of the Opal Fragments Characterized by Loss on Ignition (LOI) and Used for Calibration of the LIBS Hydrogen Signal

					LOI at 1000 °C			TGA	
Fragment	Origin	Type	Initial weight (mg)	Vacuum loss (wt%)	Total Loss (wt%)	Since Vacuum (wt%)	Error (wt%)	Total Loss (wt%)	Error (wt%)
766	Pedro II, Piauí, Brazil	Opal-A	48.5	0.1	6.2	6.1	1.1		
1039	Mintabie, Australia	Opal-A	53.3	0.9	6.3	5.4	1.0		
1040	Coober Peddy, Australia	Opal-A	103.3	0.2	7.5	7.3	0.5	7.3	0.17
1553	Mt Davis, Australia	Chalcedony	40.8	0.0	1.7	1.7	1.2	0.9	0.02
1085	New Maternal, Argentina	Opal-CT	74.6	0.2	5.7	5.5	0.7		
1547	Peru	Opal-CT	90.5	0.5	3.4	2.9	0.3		
1549		Opal-CT	23.1	1.3	4.7	3.4	2.3		
1543b	San Martin, Jalisco, Mexico	Opal-CT	35.7	0.0	9.2	9.2	1.5	9.3	0.27
1543c	San Martin, Jalisco, Mexico	Opal-CT	89.9	0.3	8.3	8.0	0.6		
1552d	Nayarit, Guadalupana, Mexico	Opal-CT	36.6	0.3	9.3	9.0	1.5		
WT86	Wegel Tena, Ethiopia	Opal-CT	99.0	3.3	5.4	2.1	0.6	6.3	1.40

Note. Weight loss observed after exposure to vacuum is indicated. The LOI result at 1000 °C for ~20 hr is shown with loss compared to initial weight ("total loss") and loss compared to weight during vacuum ("since vacuum"). The latter is used as best estimate of water content during the LIBS analyses. In addition, TGA total loss is indicated for the corresponding samples.

gas simulant in the chamber, pressure was carefully monitored. Pressure remained stable within 0.02 mbar during our analyses.

In order to estimate the actual sample water content during the laboratory LIBS analyses performed at 8 mbar of Martian gas and after exposure to vacuum, the fragments were first weighed using a microscale before exposure to vacuum (Table 1). Then, after the LIBS analyses, each fragment was weighed within 3 min after reexposure to the laboratory atmosphere. The opal weight was then monitored as a function of time for at least 15 min. If any water readsorption was observed during that time, the measured weight gain rate was used to extrapolate back to the actual lower sample weight during the LIBS analyses, before reexposure to the atmosphere. Total water content of the samples was determined using loss on ignition (LOI) in air at 1000 °C for ~20 hr. The weight difference after LIBS was subtracted from the sample weight loss from LOI to estimate the actual sample water content during LIBS analyses (Table 1).

To better understand weight loss as a function of temperature, and as an independent measurement for the water content obtained with the LOI and weighting protocol, thermogravimetric analyses (TGA) were performed on four of the samples using additional fragments (Figure 1) TGA were carried out using a Setaram Setsys 16/18 at the University of Technology, Sydney. Large pieces from 29 to 85 mg were placed in a platinum crucible. Samples were heated at a rate of 2 °C/min from room temperature to 1100 °C in an air atmosphere flowing at 20 ml/min. The baseline was subtracted point by point using blank data under the same conditions. For each sample, three runs have been performed to estimate the repeatability error of the experiments.

In order to test the evolution of hydrogen signal intensity of opal when mixed with a bedrock material, we prepared mixtures between a reference opal sample of known, high water content, and a nominally anhydrous basalt from Skjaldbreiður, Iceland (2709SKA). LOI of the basalt powder at 1000 °C for 20 hr yielded a volatile content <0.1 wt%. The opal sample 1040 was crushed into powder and mixed with the basalt in various proportions from basalt-only to 25, 50, 75, and 100 wt% opal. The mixtures were turned into pellets and analyzed by LIBS using the same protocol as for the opal fragments. The water content of each mixture pellet was calculated by relative proportions of the opal 1040, containing 7.3 ± 0.5 wt% water when placed under vacuum in the chamber (Table 1), and the basalt. Finally, a fragment of amethyst was also analyzed along with opal samples using the LIBS setup. Amethyst, a variety of quartz, is a nominally anhydrous form of silica and is used here as a blank sample to confirm the absence of atmospheric contribution to the hydrogen signal and any interference of the LIBS silicon signal for low hydrogen contents. Indeed, LIBS spectra from amethyst and basalt samples indicate the absence of any significant interference issue or atmospheric contribution with the protocol used (Figure S1).

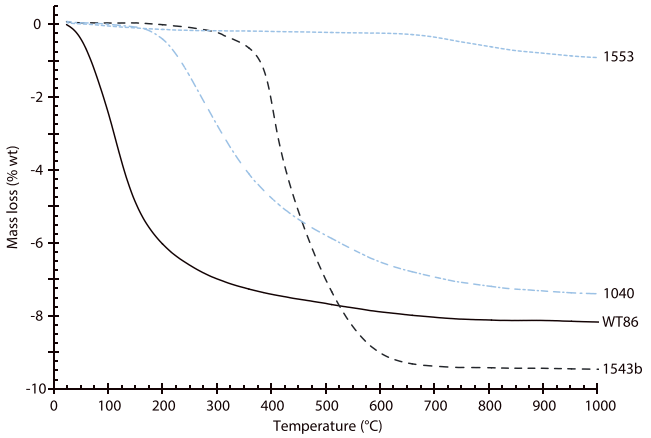

Figure 1. Thermogravimetric analyses performed on a subset of the samples used for calibration. 1553: chalcedony. 1040, WT86, and 1543b: opal.

2.3. LIBS Data Collection and Processing

Each sample was analyzed by LIBS at three locations to test homogeneity of samples. For each location a series of 150 shots at 3 Hz was acquired to test the shot-to-shot variability of the hydrogen signal. As discussed in Rapin et al. (2017a) the first 30 shots can be used to compare with standard Martian data, which is acquired using series of 30 shots on each point. In addition, the five first shots are discarded to avoid effects related to the surface on the hydrogen signal, as described in Rapin et al. (2017a). This is also a standard protocol for Martian data processing, as the five first shots help clean the ubiquitous dust cover present on rocks naturally exposed at the surface (Maurice et al., 2016). Therefore, the LIBS signal used for each analyzed location is the average spectrum of 25 shots from the 5th to 30th.

The hydrogen signal was obtained from the spectra by fitting the Balmer alpha emission peak at 656.6 nm. The processing used for both laboratory and Martian spectra is described in Rapin et al. (2017a) and summarized here. It includes a multi-Lorentz fitting method to extract the hydrogen peak area from the interference with a nearby carbon peak and a linear baseline removal. The area of the carbon peak (C I at 247.9 nm), related to the breakdown of the atmospheric CO_2, and the area of the oxygen triplet forming a single peak (O I at 778.5, 778.6 and 778.8 nm) also partly related to the atmosphere, are used for normalization of the hydrogen signal. Signal normalization, which here consists of dividing the hydrogen peak area by the carbon peak area, is important to compensate for undesired variations of the LIBS signal due to different parameters (for instance, laser-target coupling, laser focus, and distance to target). Normalization to both the carbon and oxygen peaks was proven to be the most efficient normalization proxies for the hydrogen signal. Finally, a correction factor is applied to the normalized signal in order to account for the difference of instrument response between the laboratory and flight model instruments (Rapin et al., 2017a).

3. Results

3.1. Experimental

As shown in Table 1, our samples have various water contents based on LOI results: 3.4–9.2 wt% for opals and 1.7 wt% for the chalcedony fragment. The subset of TGA total water content results are consistent with the total water losses measured by LOI. TGA curves show that the temperature of water loss varies substantially from sample to sample (Figure 1). The opals also show different behaviors related to their exposure to vacuum. While most (7 of 10) opal samples resisted water loss, 3 of them exhibited a significant loss: samples WT86, 1549, and 1039, which lost, 61%, 28% and 15%, respectively, of their initial water content (Table 1). After reexposure to the atmosphere, the weight gain was observed at a rate of about 0.06 wt% per minute for opal WT86 (Figure 2). These data highlight the ability of some opals to release water at low pressure, while others are more stable. It also shows the necessity of monitoring the opal water gain shortly after the LIBS measurements at low pressure in order to estimate the actual water content during the LIBS analyses.

Figure 3 shows that the normalized LIBS hydrogen peak area is linearly proportional to water content in our samples for opal, chalcedony, quartz, or opal-basalt pellet mixtures. Our results also correctly fit with the calibration curve obtained using calcium and magnesium sulfates, hydroxyapatites, and hydrated basalt samples (Rapin et al., 2017a). This behavior suggests that the calibration of the hydrogen signal is not dependent on chemical matrices (including mixtures with basaltic material) and that it is a robust tool to estimate water content of a great variety of minerals, including silica-rich samples on Mars.

3.2. Description of Gale Crater Observations

At Gale crater, the high-silica sedimentary rocks were observed in two geological settings: first, in the Murray lacustrine mudstone and second, within the unconformably overlying Stimson eolian sandstone in the form of light-toned halos along fractures (Figure 4). The high-silica Murray mudstone was sampled by the rover drill at a location named Buckskin. Analysis by the CheMin instrument revealed the presence of ~60 wt% amorphous components and ~40 wt% crystalline minerals; 34.1 wt% of the crystalline component is

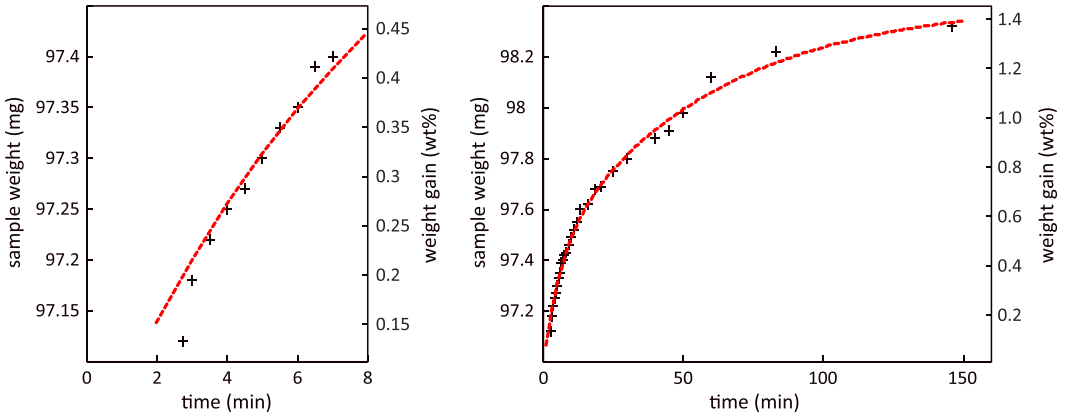

Figure 2. Monitoring of weight gain of opal sample WT86 with time after vacuum test upon reexposure to the atmosphere. The curve fit corresponds to a water adsorption kinetic model as given in (Muster et al., 2001) for silica particles $A = A_0\left(1 - e^{-k_0 t}\right) + A_c\left(1 - e^{-k_c t}\right)$ with fitted parameters A_0 (0.44 wt%) adsorption due to specific interactions and A_c (1.04 wt%) due to condensation, and k_0 (0.16/min) and k_c (0.017/min) as corresponding rate constants.

tridymite, hypothesized to be of detrital origin (Morris et al., 2016; Table 2). The amorphous components, forming a broad hump in the diffraction pattern, could be modeled by the presence of mostly opal-A or high-silica glass (~33 wt% of the total sample) and some amount of opal-CT (~6 wt%; Morris et al., 2016; Rampe et al., 2017).

In the Stimson sandstone, the light-toned halos were sampled by the drill at two locations named Greenhorn and Lubango. CheMin analyses revealed an increase in the abundance of X-ray amorphous material (up to 73 wt% in Lubango) and a decrease in igneous mineral content, compared to drill samples obtained in the surrounding, less altered sandstone at Big Sky and Okoruso (Yen et al., 2017; Table 2). For the light-toned halo samples, the amorphous components were modeled as opal-A or high-silica glass, like rhyolitic glass, which both fit the broad hump observed. Opal-CT was not identified on the diffraction pattern (Yen et al., 2017); therefore, it may be present but only in amounts below the detection limit estimated at ~3 wt% in these samples.

The ChemCam instrument was used extensively to analyze the corresponding sedimentary rocks, within the drill holes and all around, sampling 2735 LIBS observation points on 354 different targets in the area. This data set was treated as described by Frydenvang et al. (2017) to remove points related to float rocks or soils based on images, or diagenetic features of distinct composition such as Ca-sulfate veins. While the unaltered Stimson sandstone shows an average basaltic composition, an increase of SiO_2 content up to ~90 wt%

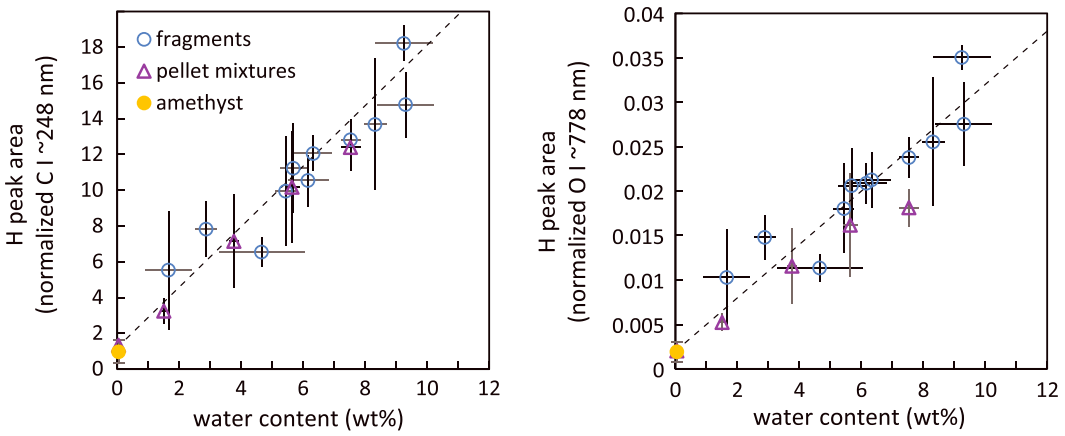

Figure 3. Hydrogen peak area normalized to (top) carbon at 247.9 nm or (bottom) oxygen at ~778 nm as a function of sample water content. It includes data from opal and chalcedony sample fragments (Table 1), pellet mixtures, and amethyst fragment. The dashed line represents the linear hydrogen calibration curve obtained using a greater variety of samples (basalts, sulfates, and phosphates; Rapin et al., 2017a).

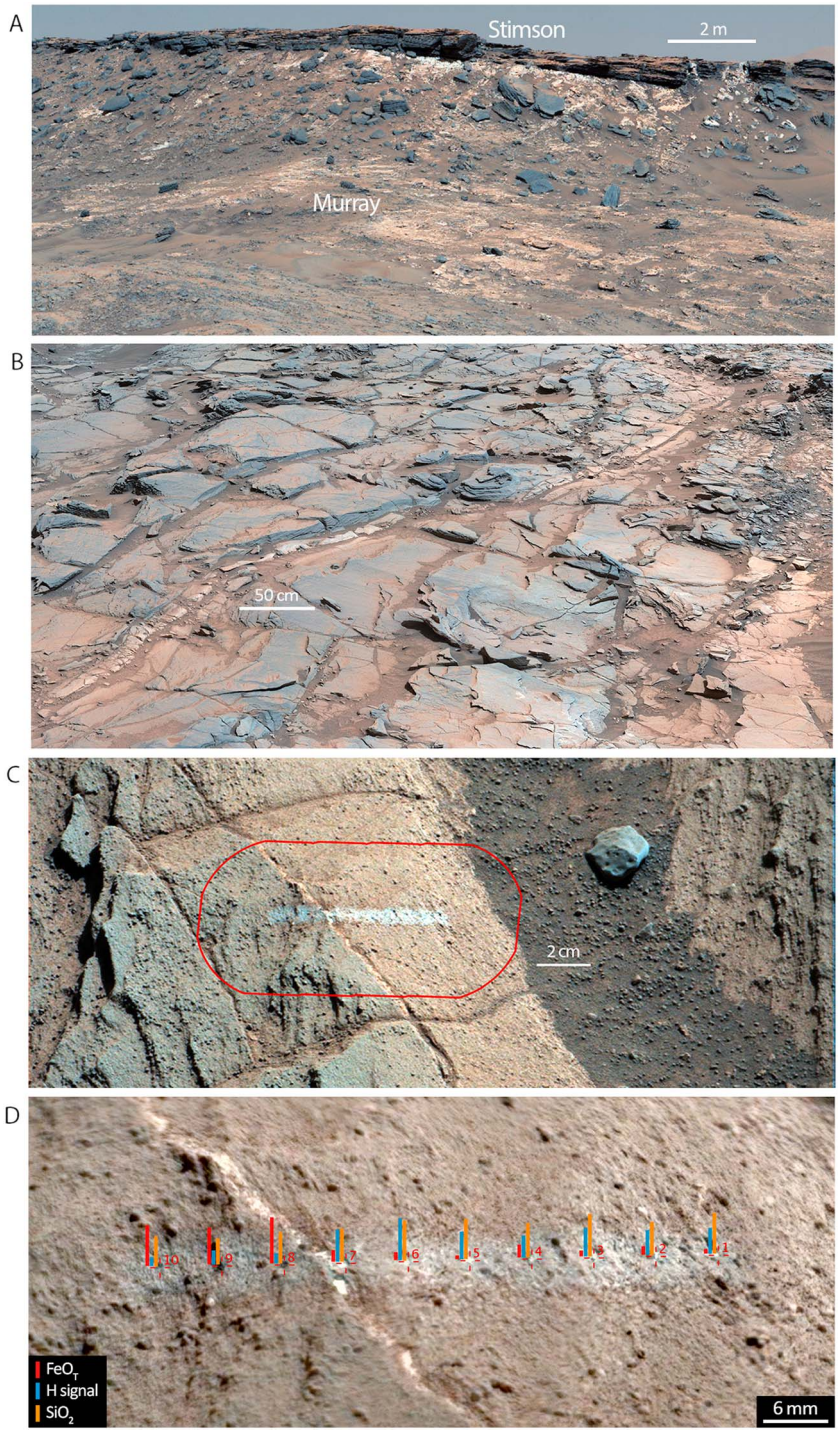

Figure 4. Context images from meter scale outcrop to submillimeter size LIBS analyses. (a) Stimson sandstone with cross-cutting alteration halos on top of the Murray mudstone (Mastcam-100 mosaic obtained on sol 1267). (b) Fracture-associated halos as observed from above the Stimson formation (mcam04766, sol 1085). (c) Context Mastcam-100 image for the ChemCam target Iona, sol 1300. (d) ChemCam RMI mosaic detail, merged with a corresponding Mastcam image to provide color, and including annotations of the 10 LIBS analyses with bars reflecting the H signal (blue), the SiO_2 (orange), and FeO_T (red) contents.

Table 2
Relevant Mineralogy Along With Silica and Water Content of the Drill Samples as Measured by ChemCam and SAM (in wt%)

			Buckskin[a]	Big Sky[b]	Okoruso[b]	Greenhorn[b]	Lubango[b]
Unit			Murray	Stimson		Stimson halos	
Granulometry			mudstone	Sandstone			
Mineralogy (wt%)	Tridymite		17.1 ± 1.0				
	Cristobalite		3 ± 0.4				
	Quartz			1.4 ± 0.3	0.9 ± 0.3	0.8 ± 0.2	0.9 ± 0.2
	Anhydrite		0.7 ± 0.2	1.2 ± 0.3	0.5 ± 0.4	5.6 ± 0.3	3.3 ± 0.2
	Bassanite				0.8 ± 0.4	1.4 ± 0.3	2.4 ± 0.3
	Gypsum						0.6 ± 0.2
	Amorphous		60[e]	20 ± 10	35 ± 15	65 ± 20	73 ± 20
Chemistry (wt%)	APXS (renormalized)	SiO_2 (bulk)	73.9[e]	42.4	43.8	51.6	57.4
		SiO_2 (amorphous)[c]	46.2[e]	6.0 ± 4.4	15.0 ± 6.7	40.9 ± 6.5	47.2 ± 7.5
	ChemCam	H_2O (bulk)	4.0 ± 1.3	1.4 ± 0.5	2.9 ± 1.3	3.2 ± 1.0	4.0 ± 1.2
		H_2O (opal only)[d]	8.0 ± 2.6	-	-	7.1 ± 2.3	7.3 ± 2.4
	SAM H_2O release		1.8 ± 0.6	1.1 ± 0.4	-	0.9 ± 0.3	-

Note. Bulk SiO_2 abundance from APXS data renormalized to include the ChemCam water content estimate. The uncertainties on amorphous silica abundances are propagated from the uncertainty of the amorphous component abundances. The uncertainties on water contents include 1-sigma uncertainties related to the laboratory calibration and to the instrument response function correction factor.
Mineral abundances from the following:
[a]Morris et al. (2016). [b]Yen et al. (2017). [c]Amount of amorphous SiO_2 in the sample. [d]Opal water content assuming all the amorphous silica and water are associated with the opal phase. [e]Lower limit constrained by APXS chemistry (Morris et al., 2016).

SiO_2 is observed in the light-toned alteration halos of the sandstone. The Murray mudstones are similarly enriched in silica in the laterally extensive area where tridymite has been observed, that is, in the bulk rock rather than in halos.

3.3. Estimation of Opal Water Content on Mars

Figure 5 shows that in both the Stimson and Murray formations, the silica content estimated by ChemCam is overall positively correlated with the hydrogen signal for all targets analyzed in the area of the high-silica sedimentary rocks. As shown on the figure, a linear fit of the observed correlation points toward an average opal water content of 6.3 ± 1.4 wt%, applying the laboratory calibration to the hydrogen signal. This least squares fit assumes a linear mixture between an opal end-member and a less altered country rock. This less altered country rock end-member is fixed at the average silica content and hydrogen signal measured in the Big Sky drill hole. The silica content is anticorrelated with respect to other major elements (Frydenvang et al., 2017), and the correlation with hydrogen is observed up to ~90 wt% SiO_2 (Figure 5), so that potentially hydrated phases not related to silica are only minor. Other possible fit hypotheses may indicate slightly different average pure silica end-members exist (e.g., Figure S2). Points with silica content between 75 and 85 wt% have a corresponding average water content of 4.0 ± 0.9 wt% for Murray and 5.3 ± 1.2 wt% for Stimson (Figure S3), which at least defines lower limits for the average water content of the silica end-members mixed with the less hydrated country rock.

Given that the hydrogen signal is correlated with the silica in both the Stimson alteration halos and the tridymite-bearing Murray mudstone, the presence of opal is likely throughout the high-silica rocks. Along with opal-A, rhyolitic glass fits the X-ray diffraction data observed by CheMin (Morris et al., 2016); however, the water content of rhyolitic glasses, or other igneous high-silica glasses, usually lies in the range of 0–3 wt% depending on the volatile content and degassing history of the original magma (Newman et al., 1986; Zhang, 1999). Although such hydrated glasses could be present in the tridymite-bearing mudstone as detrital phases, they could not represent the major amorphous silica phase according to the high water content measured, which rather supports the presence of opal. Within the Stimson sandstone the hydrated amorphous silica phase is found in alteration halos along fractures. This T geologic context also excludes detrital glasses (Frydenvang et al., 2017; Yen et al., 2017).

While the hydrogen signal and silica content are correlated, scattering from the correlation is also observed. Rapin et al. (2017b) have shown that the hydrogen LIBS signal can be affected by surface texture roughness

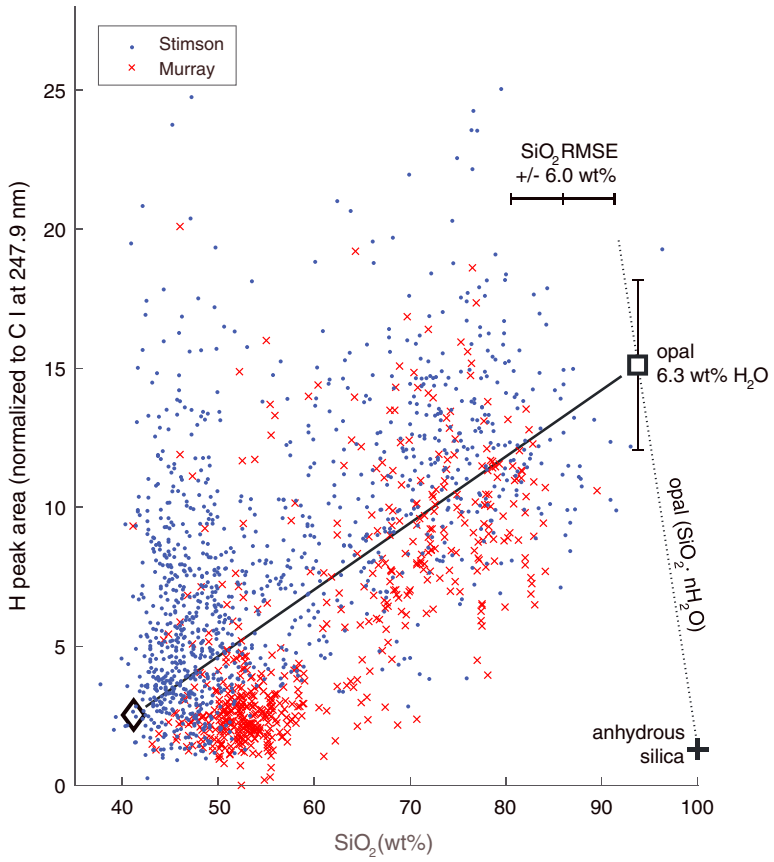

Figure 5. Hydrogen peak area normalized to carbon at 247.9 nm as a function of silica content from the bedrock in the Murray (red crosses) and Stimson (blue dots) formations. Reference signal and silica content are reported for the average data from the Big Sky drill hole corresponding to Stimson unaltered sandstone (diamond), as well as for anhydrous silica (black cross). The dotted line represents opal with varying water content according to laboratory calibration. The linear fit (solid line), crossing the Big Sky drill hole data (diamond), points toward an average opal water content of 6.3 ± 1.4 wt%. The fitted slope parameter value is 0.239 ± 0.008 (2-sigma uncertainty). The 1-sigma uncertainty on the average opal water content is mostly related to the laboratory calibration and instrument response function correction factor (Rapin et al., 2017a). The horizontal uncertainty is related to RMSE on the estimation of silica content from ChemCam spectra for $SiO_2 > 70$ wt%.

effects. The hydrogen signal has more scattered and enhanced values when the roughness scale approaches the size of the laser beam, notably near the millimeter scale typical of the sandstones. This effect is specific to the hydrogen signal and does not affect the emission of other elements (Rapin et al., 2017b). The ChemCam LIBS data from the unaltered Stimson sandstone, with approximately millimeter-sized roughness, exhibit this phenomenon by showing more pronounced scatter for higher H values (Figure 5) though the bedrock has relatively homogenous composition. Conversely, the typical Murray mudstone, with ~50 wt% SiO_2, has a significantly smoother surface texture and, as seen on the figure, yields a much less scattered hydrogen signal.

Nevertheless, in spite of the complications of roughness, the observed increase of hydrogen signal with increasing silica cannot be attributed to the effect of roughness. First, the alteration halos of the Stimson sandstone with elevated hydrogen have no visible increase of surface roughness compared to the unaltered sandstone (Figure 4d). Second, all points with significantly elevated silica (>80 wt%) show an elevated hydrogen signal, consistent with at least ~4 wt% H_2O. If the silica-enriched materials were not in fact more hydrated than the country rock, the roughness effect would only yield high hydrogen signal points randomly and still show a significant number of points with low hydrogen signal, which is not observed.

Part of the variability in the hydrogen signal can also indicate true variation of the targets' water content, as opals are known to contain variable amounts of water. Within the Stimson sandstone, no systematic variation of water content could be clearly identified in the light-toned halos from one target to another. Yet the lowest

hydrogen signal values obtained in the high-silica Murray appear slightly lower than the lowest values for the high-silica Stimson. This could be due to the presence of tridymite and cristobalite, which represent ~20 wt% of the bulk Buckskin sample (Morris et al., 2016; Table 2). But Figure 5 shows that all enrichment in silica is associated with higher hydration, suggesting that the tridymite or cristobalite in the Murray mudstone is fine-grained ($<$100 μm) and closely mixed with the opal phase. Data from the two formations were also fitted independently and show a slightly lower water content for the opal in the Murray by ~1.7 wt% compared to the Stimson (Figure S2). This difference is close to the 1-sigma uncertainty of the quantification of water content, and part of the hydrogen signal difference may be explained by variable target roughness (Rapin et al., 2017b), but it may also indicate that the opal from the two formations have distinct average water contents.

In addition to the sampling of naturally exposed rocks, whose texture somewhat impacts the hydrogen signal, ChemCam also made LIBS observations of the drill-hole walls. Because the surface of the borehole is abraded by the drill, it is relatively smooth and flat and shows less variability in the LIBS hydrogen signal (Figure S3). These measurements may therefore be used to directly estimate the hydrogen content of the sample. Table 2 shows the equivalent water content derived for each drill sample using LIBS points obtained on the drill hole walls, estimated from hydrogen peak area (see also Figure S4).

4. Discussion

ChemCam data show that silica enrichments observed at Gale crater are associated with hydrogen and consistent with an opal phase of 6.3 ± 1.4 wt% H_2O on average. These results can be compared to other instruments with different effective analytical footprints and techniques to provide complementary information related to the distribution of water in the silica-rich rocks, the nature of the opal phase, and the stability of its water.

4.1. Comparison to Bulk Mineralogy and Chemistry

For each drill sample, the crystalline mineralogy obtained by the CheMin instrument can be compared to the bulk elemental composition in order to estimate the composition of the amorphous component using a mass balance approach (e.g., Blake et al., 2013; Dehouck et al., 2014; Morris et al., 2016; or Yen et al., 2017). The APXS instrument analyzed the drill powders with a footprint of 1.7-cm diameter to provide the bulk abundance of major oxides and minor elements. ChemCam also provides elemental composition but is not quantitative on sulfur; therefore, we used APXS composition to account for the sulfate mineralogy measured by CheMin. However, the APXS is not sensitive to hydrogen, and the oxide compositions are normalized to 100% without accounting for water or hydroxyls present in the sample. The water content estimated by ChemCam for each drill sample was thus added to the oxide compositions and the mass balance recalculated to sum to 100% (see Table S1). The amorphous component is then calculated by subtraction of the composition of the crystalline phases detected by CheMin. With a mostly anhydrous crystalline component (except for small amounts of hydrated calcium sulfates), the water measured by ChemCam must predominantly reside in the amorphous component (Table 2).

At Buckskin, Greenhorn, and Lubango, the amorphous component includes 65 to 77 wt% SiO_2. If all of the silica and water of the amorphous component is attributed to an opal phase, this yields an opal water content of 8.0 and 7.1 wt% (Table 2). This estimate likely represents an upper limit of the actual opal water content because part of the water could be associated with other amorphous phases such as ferrihydrite or Fe/Mg-bearing amorphous sulfates (e.g., Dehouck et al., 2017; Sklute et al., 2015; Wang et al., 2009). However, we argue that most of the hydrogen is associated with silica, given the hydrogen-silica correlation for Murray targets observed on Figure 5, where SiO_2 increases to ~90 wt%. This shows that a significantly hydrated phase associated with other elements is unlikely or minor in the bulk samples. Upper bounds of 7.1 to 8.0 wt% H_2O derived for opal within the different drill samples (Table 2) compare well to the average water content of 6.3 ± 1.4 wt% derived from the data of all targets sampled in Stimson and Murray (Figure 5).

4.2. DAN Measurements

The DAN instrument acquired active neutron measurements along the rover's traverse through the Murray tridymite-bearing mudstone and around the light-toned halos in the Stimson sandstone. The instrument, in active mode, generates high-energy neutron pulses that interact with the near-surface materials through scattering interactions with nuclei. The DAN detector records the arrival times of thermal and epithermal

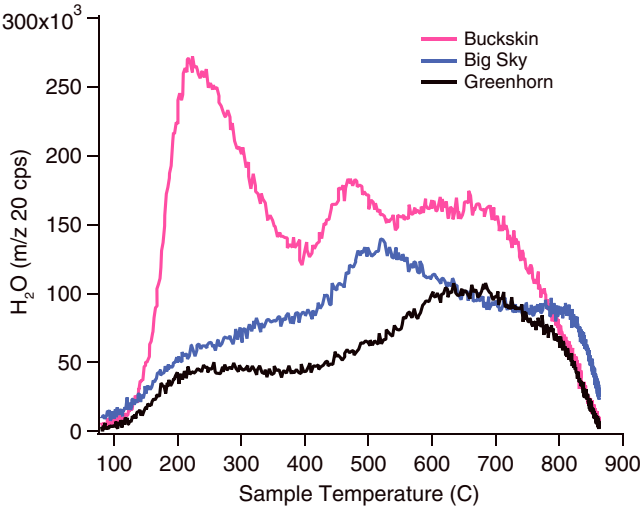

Figure 6. SAM H_2O evolved gas analysis mass spectrometry (EGA-MS) measurements from the Buckskin, Big Sky, and Greenhorn samples. Since the signal from the H_2O main mass-to-charge ratio (*m/z* 18, $H_2{}^{16}O$) was saturated, counts from an H_2O isotopologue (*m/z* 20, $H_2{}^{18}O$) are shown versus temperature to depict the H_2O signal. For more details on SAM EGA-MS analysis, see Sutter et al. (2017).

neutrons scattered back to the instrument after each neutron pulse. This time profile strongly depends on the distribution of hydrogen and other neutron-absorbing elements, for example, Fe and Cl, to depths of ~60 cm below the surface. The instrument typically samples a spherical-cap volume of ~3 m in diameter at the surface (Mitrofanov et al., 2012). Several areas with silica enrichments have been analyzed by the DAN team, including areas surrounding the drill sites of (i) Buckskin in the tridymite-bearing mudstone and (ii) Lubango/Okoruso, the altered/unaltered fracture-associated halo in the Stimson sandstone.

At Buckskin, a DAN active measurement was not performed directly over the drill site, but instead, several nearby DAN measurements were made along the rover traverse through Marias Pass. Deriving accurate hydrogen contents from these measurements requires analysis of stratigraphy and images of the drive location in order to determine correlations between the locations of the DAN measurements and contact science locations of high-silica rock. Preliminary analysis of the nearest DAN active measurement to the drill site does not provide a good statistical fit when the models assume a homogeneous distribution of Buckskin-like rock underneath the rear of the rover (Rover site 48, drive 2542). As such, ongoing efforts are aimed at modeling other Murray formation geochemical abundances derived from targets such as Elk (Sol 992), as well as other stratigraphic relationships between high-silica Murray units, which may be more representative of the bulk rock in the DAN field-of-view near the Buckskin drill site (T. S. J. Gabriel and C. Hardgrove, personal communication, September 28, 2017).

In contrast with the Buckskin drill site, a dedicated DAN active campaign was performed directly over the Lubango alteration halo and above the nearby unaltered Stimson sandstone. In particular, several "off-halo" measurements were performed in addition to a measurement directly above the Lubango drill site. Due to the complex geometry of the halo, which transected the DAN field-of-view, a geometric model of the fracture-halo was developed, with a surrounding and underlying rock composed of unaltered Stimson sandstone. Preliminary refinement of Gabriel et al. (2017) indicates a water content of 5.1 ± 1.0 wt% in the fracture halo, whereas best fit models indicate 2.0 ± 0.3 wt% water in the unaltered Stimson sandstone near the Okoruso drill site. DAN is sensitive to hydrogen regardless of the molecular bonding (OH versus H_2O), as is the case for ChemCam. The reported water content therefore represents the equivalent based on hydrogen abundance (or water equivalent hydrogen) and indicates the upper limit on water abundance in the rock. These preliminary results are consistent with water content measured independently using ChemCam at the drill locations for Greenhorn and Lubango within the halos and at Big Sky for the unaltered Stimson sandstone (Table 2).

4.3. SAM Measurements

The SAM instrument performed pyrolysis and EGA of the Buckskin and Greenhorn samples. The measurements yielded water abundances of, respectively, 1.8 ± 0.6 and 0.9 ± 0.3 wt% H_2O for these samples (Sutter et al., 2017; reported in Table 2). The release is observed over a broad range of temperatures, up to 800 °C (Figure 6). The low bulk amount of water and absence of significant release at low temperature is rather inconsistent with the observations by ChemCam and DAN. However, the results of the SAM instrument could be explained by a loss of water before the pyrolysis due to several factors. Variations of temperature during handling before SAM analysis have likely affected the samples. The Buckskin and Greenhorn drill powders were held in CHIMRA (Collection and Handling for Interior Martian Rock Analysis) for 16 and 41 Martian solar days, respectively, between drilling and delivery to SAM. Diurnal temperatures in CHIMRA are similar to those outside on the surface, but slightly higher, exposing the sample powder to lower relative humidity. Time spent in that environment could have resulted in some low-temperature water loss.

After delivery, the samples spent some time in SAM prior to EGA. The process of delivering sample portions from CHIMRA to the SAM cup took about 40 min. The temperature inside SAM at the time of delivery of the

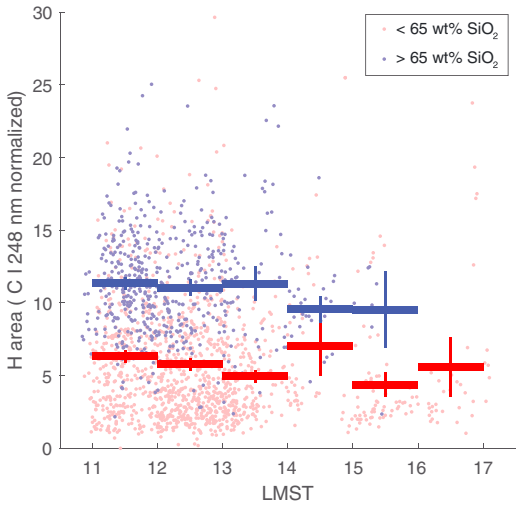

Figure 7. Hydrogen peak area normalized to carbon at 247.9 nm as a function of local mean solar time on high (blue) or low (red) silica targets within the Stimson and Murray formation. The thick horizontal segments indicate the average hydrogen signal for each time bin; the vertical error bar corresponds to the 2-sigma uncertainty and the mean value.

samples was ~20 °C. After delivery, the samples were sealed inside the pyrolysis oven until the time of the EGA experiment. Some additional hours elapsed between delivery and the experiment because delivery usually occurs during the day but SAM performs at night, and not necessarily on the same night as the delivery. The Buckskin sample was sealed in the oven for 30 hr before the start of the EGA experiment. For Greenhorn the time was about 7 hr. During those times, the oven and sample are expected to experience diurnal temperatures varying between 5 and 25 °C; however, the oven is a small sealed volume, not exposed to gas flow or open to the Martian atmosphere. Some changes in the water state in the amorphous silica of the samples could occur during this time, but it may be that other parts of the sample processing have a more significant effect. Immediately before the start of the EGA run, the samples were preheated to ~40 °C for 21 min, under a low helium flow at 25 mbar. This is a common experimental protocol for SAM (not unique to the Buckskin and Greenhorn samples), and this treatment likely contributed to loss of weakly held molecular water.

The temperature required to release most of the molecular water is known to vary significantly among opals. Figure 1, showing the TGA results for some of the opal samples used for calibration, illustrates the diversity of behaviors with peak weight-loss temperatures varying between 100 and 400 °C. Other studies reported opals releasing most of their molecular water at even lower temperatures. In particular, Segnit et al. (1965) studied opals that lost more than half of their initial water in the 50 to 70 °C temperature range. In addition, pressure influences the stability of water in opals. Experiments have shown that at room temperature, some opals will dehydrate at low pressures typical of Mars (Rice et al., 2013; Sun, 2017) or when exposed to a low partial pressure of water vapor in a desiccant (Segnit et al., 1965). As shown in Table 1, the opal samples 1549 and WT86 lost a significant amount of water when exposed to vacuum. Therefore, it is expected that during a SAM EGA on Mars opals could dehydrate at temperatures lower than observed in laboratory TGA performed under ambient pressure.

Furthermore, opal susceptibility to water release is enhanced by powdering. The rover drill turns samples into powder, and a $<$150 μm fraction is analyzed by SAM. Such grinding can significantly reduce the temperature required to release water from an opal sample compared to its bulk form (Thomas et al., 2007). In the laboratory, EGA analysis performed on powdered sample 1040 under SAM-like conditions (He flow, 25 mbar He pressures, and SAM-like temperature ramp) with simultaneous TGA showed a difference of about 2 wt% water content (H_2O release ~5.3 wt%) compared to room pressure TGA of the bulk (nonpowdered) opal sample (H_2O release 7.3 wt%; Table 1). (TGA is not possible on the SAM flight instrument but is an additional function of the SAM-like EGA laboratory instrument.)

In summary, a combination of factors related to sample preheating, low pressure, and grinding supports the scenario of opal degassing prior to SAM pyrolysis to explain the inconsistency with water contents measured by ChemCam and DAN. Crushing the Buckskin and Greenhorn samples into powder would have reduced the temperature of water release in the opal phase, and then handling and preheating led to degassing before pyrolysis. In addition, the low pressure on Mars and during pyrolysis in the SAM instrument would also lead to an overall lower water release temperature compared to terrestrial pyrolysis results from experiments at ambient pressure.

4.4. Stability of Water in the Opal Phase

The combined results of ChemCam, DAN, and SAM highlight a specific behavior of the water held in the opal phase. Water contained in opal, estimated at 6.3 ± 1.4 wt% by the ChemCam instrument, is present in the rocks exposed to current low pressure conditions at the surface with diurnal temperatures that can vary between −95 and ~15 °C (Vasavada et al., 2017) and water vapor mixing ratio of 10–80 ppmv (Savijärvi et al., 2016). Based on the different water contents measured by SAM compared to DAN and ChemCam, the opal phase within the Buckskin and Greenhorn sample likely lost 50–70% of the initial water due to handling and preheating (Table 2). The 1.8 ± 0.6 wt% water evolved from the Buckskin sample shows a broad loss

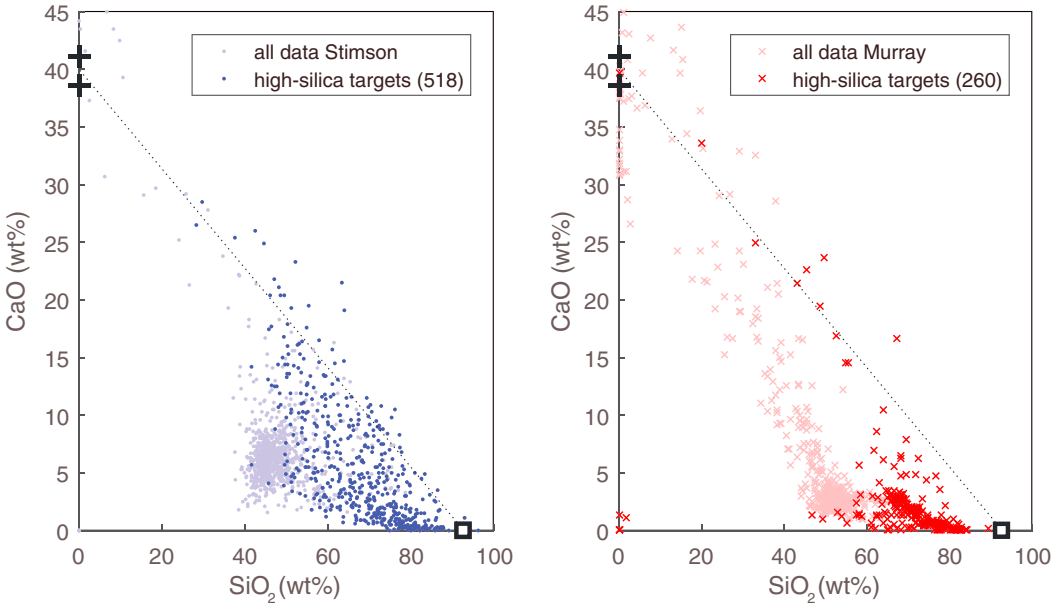

Figure 8. Silica content as a function of calcium oxide content for targets of the Stimson and Murray formations. Data from targets, which include one or several points with more than 65 wt% SiO_2 and less than 3 wt% CaO, are represented for the Stimson (bold blue dots) and Murray (bold red crosses). The total number of points from these targets is shown in the legend: 518 for Stimson and 260 for Murray. The remaining target data are shown in lighter color (Stimson: pale blue dots, Murray: pale red crosses). Note that this data set deliberately includes all points, whereas data shown on Figure 5 were classified to remove points with a contribution from Ca-sulfates (Frydenvang et al., 2017). Reference compositions of opal with 6 wt% water (black square), as well as anhydrite -$CaSO_4$- and bassanite -$CaSO_4 \times 0.5H_2O$- (black crosses), are shown along with mixing trend (dotted line).

peak at ~200 °C, which could represent the fraction of the water adsorbed in the opal, which was not fully degassed during handling and preheating (Figure 6). The Greenhorn sample does not exhibit a loss peak at temperatures below 400 °C and evolved an even lower total water content (0.9 ± 0.3 wt%), suggesting that almost no adsorbed water remained in the opal. Most of the opal water observed by ChemCam is molecular water either superficially bound (released below 150 °C; Thomas et al., 2015) and/or in pores (released in the 150–250 °C range; Thomas et al., 2015). A broad release above 600 °C could instead correspond to strongly bound silanols. The peak in the 450–500 °C range, however, may not be related to opal but could result from minor jarosite (Sutter et al., 2017).

Given that most of the adsorbed water may have been lost due to handling and preheating at ~40 °C, the opal phase exposed at the surface of Mars appears to be close to its dehydration temperature at daytime peak temperatures on Mars. This suggests that part of this water could be exchanged with the atmosphere due to diurnal temperature and humidity variations. Yet Figure 7 shows that no variation of the ChemCam hydrogen signal from the opal-bearing rocks is observed during the day. However, most measurements were performed near noon, starting at 11:00 LMST, and no nighttime or dusk measurements were performed on the high silica rocks. Therefore, some degree of diurnal exchange still cannot be excluded and additional measurements would be needed to assess this process.

In addition, the opal could be dehydrating at the surface as it is being exhumed and exposed to current climate by erosion, forming a hydration gradient from the surface downward. The preliminary result from DAN data suggests that the water content over the DAN footprint going down to ~60 cm in depth in the halo may indeed be slightly higher than the water content measured at the surface by ChemCam (Table 2). Refinement of the DAN geometric model will help better constrain the hypothesis of a hydration gradient in the opal-bearing rocks.

4.5. Formation and Diagenesis

The formation of opal within light-toned halos along fractures is unambiguously related to diagenetic fluid alteration after lithification of both the Murray and Stimson formations. Frydenvang et al. (2017) proposed

that silica was mostly mobilized by neutral to alkaline fluids from the Murray tridymitic mudstone and deposited into the sandstone following fractures. Yen et al. (2017) argued that acidic leaching should have passively enriched the sedimentary rocks first, and subsequent mobilization and deposition of silica also occurred by rather neutral pH fluids. Yet both studies acknowledged that a complex sequence of fluid events likely occurred to account for the geochemistry observed.

The light-toned alteration halos are also associated with calcium sulfates as shown by the presence of substantial anhydrite (5.3 and 3.1 wt%), bassanite (1.3 and 2.1 wt%), and even some gypsum, in the Greenhorn and Lubango drill samples, compared to the much sparser occurrence of these phases in the unaltered sandstone (e.g., Yen et al., 2017; Table 2). Calcium sulfates are widespread in the Murray formation explored by Curiosity in the form of fracture-fill veins, with millimeter- to centimeter-scale thickness (Nachon et al., 2014, 2017). These veins are predominantly composed of bassanite from the dehydration of gypsum (Rapin et al., 2016), while the silica in the halos is rather associated with anhydrite (Yen et al., 2017), which requires higher temperature or high salinity to form (Freyer & Voigt, 2003; Marion et al., 2016). Calcium sulfate veins are also observed in the Stimson sandstone and, in some cases, form boundaries separating the altered from the unaltered sandstone showing that the silica deposition was blocked by the filled fracture (Figure 4c). This indicates that sulfate-filled fractures predated the formation of the diagenetic opal.

Within the alteration halos, no visible vein or veinlets can be identified to account for the bulk calcium sulfate mineralogy. Figure 8 shows a significant number of points spread along the mixing line between opal and the end-member calcium sulfates. Given the ChemCam LIBS footprint size, such points indicate that rather pure calcium sulfate and silica assemblages can be found within the Stimson halos at the scale of ~400 μm (in 36% of points). This association with calcium sulfate is not as common for the opal present in the tridymite-bearing Murray mudstone (only 8% of points; Figure 8), which suggests that the precipitation of the two phases from the diagenetic fluids likely occurred in multiple stages. The proximity of the opals found in the tridymitic Murray mudstone and in the halos suggests that it could have formed from the same diagenetic episode. However, its variable association with calcium sulfates, the slight difference of opal water content (Figure S2), and degassing behavior (Figure 6) between the Murray and Stimson may indicate distinct opals formed at different times. The contact relationships between opal bearing units observed to date in the Murray and Stimson do not resolve the question (Frydenvang et al., 2017; Yen et al., 2017).

The exact timing for the formation of the opal is not well known. The emplacement, lithification of the Mt Sharp sedimentary rocks, and their subsequent erosion and exposure down to a level near the present surface should have taken place during the Hesperian by 3.3 to 3.2 billion years ago according to crater counting of crater floor units (Grant et al., 2014; Grotzinger et al., 2015; Thomson et al., 2011). The opal found in the halos probably formed late during this Hesperian time frame. In particular, it must have formed after the lithification of the Stimson formation lying unconformably over the Murray formation, but it is not clear how much erosion could have occurred in the meantime. Opal in the Murray mudstone might be older, possibly forming in an early diagenetic process or as part of the initial lake sediments. In addition, the presence of small amounts of opal-CT in the Murray mudstone, but not in the halos, may indicate some initial opal-A of the mudstone underwent progressive diagenesis not observed in the alteration halos. Opal formation in the halos during the Amazonian is also possible, as evidence on Mars shows that excursions from cold and arid conditions have taken place and could have permitted the presence of liquid water in the near subsurface (Fairén et al., 2009; McCubbin et al., 2010), and indeed, it has been suggested that alluvial fans in Gale crater and the surrounding region have been active in the Amazonian (Ehlmann & Buz, 2015; Grant et al., 2014; Palucis et al., 2014, 2016).

On Earth, the diagenesis of opal-A leads to the formation of opal-CT and microcrystalline quartz though a dissolution-precipitation processes (Williams & Crerar, 1985), even with little to no burial (Lynne et al., 2005). Opal-A is predominantly observed at Gale crater with only low amounts of opal-CT measured in the Murray mudstone (Morris et al., 2016; Rampe et al., 2017), not always associated with opal-A, and also without any significant quartz. Therefore, only very limited diagenesis could have occurred after the formation of the alteration halos, so the formation of the opal observed at Gale crater likely represents the last significant water-rock interaction in the sedimentary rocks. In terrestrial settings, opal-A can transform into opal-CT and subsequently into microcrystalline quartz within thousands of years (Lynne et al., 2005). However, some occurrences of opal-A are dated at several tens of million years (as the Australian opals; Rey, 2013). There is no

record of opal-A preserved over several hundred million years; yet, in contrast to several billion years the opal-A has been preserved at Gale crater.

Multiple factors are involved in the transformation of opal-A and opal-CT. Several studies show that opal-A transformation may occur between 0 and 50 °C (Botz & Bohrmann, 1991; Matheney & Knauth, 1993; Williams & Crerar, 1985). Chemical and mineralogical factors, such as the fluid aluminum or magnesium content, and also the association with clays or carbonate minerals, as well as particle coatings, may also affect the processes and rates of dissolution/reprecipitation (Hinman, 1998; Kastner et al., 1977; Rickert et al., 2002). All these controlling factors, which are unknown or hardly quantified on Mars, prevent an estimate of the duration of fluid flow following the precipitation of opal. In all cases, the presence of liquid water is a requirement for the diagenesis, thus suggesting that limited water-rock interaction has occurred since formation, which precluded the diagenesis of opal at Gale crater, as elsewhere on Mars (Tosca & Knoll, 2009).

5. Conclusion

The Curiosity rover payload at Gale crater offers a new opportunity to characterize silica enrichments discovered in situ. Using laboratory experiments, we have shown that the ChemCam LIBS hydrogen signal can be used to quantify the water content of opals. On Mars, the X-ray amorphous nature of the silica and the correlation of the silica content with the hydrogen signal observed by ChemCam indicate an opal-A phase with 6.3 ± 1.4 wt% water on average. The presence of substantial, elevated water content in silica-rich rocks is corroborated by the DAN instrument measurements. The pyrolysis experiments performed by SAM show that much of the water in the opals was likely released at relatively low temperature during handling of the samples.

Opal found in the fracture-associated halos and in the tridymite-bearing Murray mudstone appears to have formed from diagenetic fluids. Its relation to calcium sulfates, present within the silica enrichments but also in fracture fills, suggests that multiple stages of fluid alteration have occurred. The opal preserved significant water content and mostly remained in the opal-A form, which shows that only limited diagenesis took place after formation. Such preservation, likely over billions of years during the Amazonian, suggests that the opal forming event represents the last significant water-rock interaction in these sedimentary rocks.

Acknowledgments

The research was funded at Caltech by the Division of Geological and Planetary Sciences Postdoctoral Fellowship and supported by a NASA MSL Participating Scientist Program grant to B. L. Ehlmann. The work performed at Université Paul Sabatier was part of a PhD thesis (Rapin, 2016), and laboratory LIBS experiments were conducted at Institut de Recherche en Astrophysique et Planétologie (IRAP) with support from CNES. MSL/ChemCam U.S. operations were funded by the NASA Mars Exploration Program. Funding for ChemCam operations in France was provided by CNES. The authors gratefully acknowledge the support of all of the people at NASA-JPL involved in making MSL a successful mission. We also thank two anonymous reviewers for their helpful comments. We acknowledge the Agence Nationale de la Recherche (ANR) under the program ANR-16-CE31-0012 entitled "Mars-Prime" for helping collaborative efforts in this study. The authors thankfully recognize the help of Paul Thomas, from the University of Technology, Sydney, for TGA on opals. A. C. M. thanks NASA's MSL Participating Scientist program for supporting this effort. All data collected on Mars by MSL/Curiosity used in this study are available on the PDS (Planetary Data System) at pds.nasa.gov. Data shown in Figures 1 and 2 are accessible in the supporting information.

References

Anderson, J. H., & Wickersheim, K. A. (1964). Near infrared characterization of water and hydroxyl groups on silica surfaces. *Surface Science*, *2*, 252–260. https://doi.org/10.1016/0039-6028(64)90064-0

Audouard, J., Poulet, F., Vincendon, M., Milliken, R. E., Jouglet, D., Bibring, J.-P., et al. (2014). Water in the Martian regolith from OMEGA/Mars Express. *Journal of Geophysical Research: Planets*, *119*, 1969–1989. https://doi.org/10.1002/2014JE004649

Bandfield, J. L., Amador, E. S., & Thomas, N. H. (2013). Extensive hydrated silica materials in western Hellas Basin, Mars. *Icarus*, *226*(2), 1489–1498. https://doi.org/10.1016/j.icarus.2013.08.005

Behl, R. J. (2011). Chert spheroids of the Monterey formation, California (USA): Early-diagenetic structures of bedded siliceous deposits. *Sedimentology*, *58*(2), 325–351. https://doi.org/10.1111/j.1365-3091.2010.01165.x

Blake, D. F., Morris, R. V., Kocurek, G., Morrison, S. M., Downs, R. T., Bish, D., et al. (2013). Curiosity at Gale crater, Mars: Characterization and analysis of the Rocknest sand shadow. *Science*, *341*(6153), 1239505. https://doi.org/10.1126/science.1239505

Boboň, M., Christy, A. A., Kluvanec, D., & Illášová, L. (2011). State of water molecules and silanol groups in opal minerals: A near infrared spectroscopic study of opals from Slovakia. *Physics and Chemistry of Minerals*, *38*(10), 809–818. https://doi.org/10.1007/s00269-011-0453-0

Botz, R., & Bohrmann, G. (1991). Low-temperature opal-CT precipitation in Antarctic deep-sea sediments: Evidence from oxygen isotopes. *Earth and Planetary Science Letters*, *107*(3–4), 612–617. https://doi.org/10.1016/0012-821X(91)90105-Q

Chauviré, B., Rondeau, B., & Mangold, N. (2017). Near infrared signature of opal and chalcedony as a proxy for their structure and formation conditions. *European Journal of Mineralogy*. https://doi.org/10.1127/ejm/2017/0029-2614

Chauviré, B., Rondeau, B., Mazzero, F., & Ayalew, D. (2017). The precious opal deposit at Wegel Tena, Ethiopia: Formation via successive oedogenesis events. *The Canadian Mineralogist*, *55*(4), 701–723. https://doi.org/10.3749/canmin.1700010

Dehouck, E., McLennan, S. M., Meslin, P.-Y., & Cousin, A. (2014). Constraints on abundance, composition, and nature of X-ray amorphous components of soils and rocks at Gale crater, Mars. *Journal of Geophysical Research: Planets*, *119*, 2640–2657. https://doi.org/10.1002/2014JE004716

Dehouck, E., McLennan, S. M., Sklute, E. C., & Dyar, M. D. (2017). Stability and fate of ferrihydrite during episodes of water/rock interactions on early Mars: An experimental approach. *Journal of Geophysical Research: Planets*, *122*, 358–382. https://doi.org/10.1002/2016JE005222

Ehlmann, B. L., & Buz, J. (2015). Mineralogy and fluvial history of the watersheds of Gale, Knobel, and Sharp craters: A regional context for the Mars Science Laboratory Curiosity's exploration. *Geophysical Research Letters*, *42*, 264–273. https://doi.org/10.1002/2014GL062553

Ehlmann, B. L., Mustard, J. F., Swayze, G. A., Clark, R. N., Bishop, J. L., Poulet, F., et al. (2009). Identification of hydrated silicate minerals on Mars using MRO-CRISM: Geologic context near Nili Fossae and implications for aqueous alteration. *Journal of Geophysical Research*, *114*, E00D08. https://doi.org/10.1029/2009JE003339

Fairén, A. G., Schulze-Makuch, D., Rodríguez, A. P., Fink, W., Davila, A. F., Uceda, E. R., et al. (2009). Evidence for Amazonian acidic liquid water on Mars—A reinterpretation of MER mission results. *Planetary and Space Science*, *57*(3), 276–287. https://doi.org/10.1016/j.pss.2008.11.008

Flörke, O. W., Graetsch, H., Röller, K., Martin, B., & Wirth, R. (1991). Nomenclature of micro-and non-crystalline silica minerals. *Neues Jahrbuch Für Mineralogie, Abhandlungen*, *163*, 19–42.

Flörke, O. W., Köhler-Herbertz, B., Langer, K., & Tönges, I. (1982). Water in microcrystalline quartz of volcanic origin: Agates. *Contributions to Mineralogy and Petrology*, *80*(4), 324–333. https://doi.org/10.1007/BF00378005

Fraeman, A. A., Ehlmann, B. L., Arvidson, R. E., Edwards, C. S., Grotzinger, J. P., Milliken, R. E., et al. (2016). The stratigraphy and evolution of lower Mount Sharp from spectral, morphological, and thermophysical orbital data sets. *Journal of Geophysical Research: Planets*, *121*, 1713–1736. https://doi.org/10.1002/2016JE005095

Freyer, D., & Voigt, W. (2003). Crystallization and phase stability of $CaSO_4$ and $CaSO_4$-based salts. *Monatshefte Für Chemie/Chemical Monthly*, *134*(5), 693–719. https://doi.org/10.1007/s00706-003-0590-3

Frydenvang, J., Gasda, P. J., Hurowitz, J. A., Grotzinger, J. P., Wiens, R. C., Newsom, H. E., et al. (2017). Diagenetic silica enrichment and late-stage groundwater activity in Gale crater, Mars. *Geophysical Research Letters*, *44*, 4716–4724. https://doi.org/10.1002/2017GL073323

Gabriel, T. S. J., Hardgrove, C., Litvak, M., Mitrofanov, I., Boynton, W. V., Fedosov, F., et al. (2017). Bulk hydrogen content of high-silica rocks in Gale crater with the active dynamic albedo of neutrons experiment (p. 2875). Presented at the 48th Lunar and Planetary Science Conference.

Gaillou, E., Fritsch, E., Aguilar-Reyes, B., Rondeau, B., Post, J., Barreau, A., & Ostroumov, M. (2008). Common gem opal: An investigation of micro- to nano-structure. *American Mineralogist*, *93*(11–12), 1865–1873. https://doi.org/10.2138/am.2008.2518

Glotch, T. D., Bandfield, J. L., Christensen, P. R., Calvin, W. M., McLennan, S. M., Clark, B. C., et al. (2006). Mineralogy of the light-toned outcrop at Meridiani Planum as seen by the Miniature Thermal Emission Spectrometer and implications for its formation. *Journal of Geophysical Research*, *111*, E12S03. https://doi.org/10.1029/2005JE002672

Goryniuk, M. C., Rivard, B. A., & Jones, B. (2004). The reflectance spectra of opal-A (0.5–25 μm) from the Taupo Volcanic Zone: Spectra that may identify hydrothermal systems on planetary surfaces. *Geophysical Research Letters*, *31*, L24701. https://doi.org/10.1029/2004GL021481

Graetsch, H., Flörke, O. W., & Miehe, G. (1985). The nature of water in chalcedony and opal-C from Brazilian agate geodes. *Physics and Chemistry of Minerals*, *12*(5), 300–306. https://doi.org/10.1007/BF00310343

Graetsch, H., Gies, H., & Topalović, I. (1994). NMR, XRD and IR study on microcrystalline opals. *Physics and Chemistry of Minerals*, *21*(3), 166–175. https://doi.org/10.1007/BF00203147

Grant, J. A., Wilson, S. A., Mangold, N., Calef, F., & Grotzinger, J. P. (2014). The timing of alluvial activity in Gale crater, Mars. *Geophysical Research Letters*, *41*, 1142–1149. https://doi.org/10.1002/2013GL058909

Grotzinger, J. P., Gupta, S., Malin, M. C., Rubin, D. M., Schieber, J., Siebach, K., et al. (2015). Deposition, exhumation, and paleoclimate of an ancient lake deposit, Gale crater, Mars. *Science*, *350*(6257), aac7575. https://doi.org/10.1126/science

Hinman, N. W. (1998). Sequences of silica phase transitions: Effects of Na, Mg, K, Al, and Fe ions. *Marine Geology*, *147*(1-4), 13–24. https://doi.org/10.1016/S0025-3227(98)00002-4

Jones, B., & Renaut, R. W. (2004). Water content of opal-A: Implications for the origin of laminae in geyserite and sinter. *Journal of Sedimentary Research*, *74*(1), 117–128. https://doi.org/10.1306/052403740117

Kastner, M., Keene, J. B., & Gieskes, J. M. (1977). Diagenesis of siliceous oozes—I. Chemical controls on the rate of opal-A to opal-CT transformation—An experimental study. *Geochimica et Cosmochimica Acta*, *41*(8), 1041–1059. https://doi.org/10.1016/0016-7037(77)90099-0

Langer, K., & Flörke, O. W. (1974). Near infrared absorption spectra (4000–9000 cm- 1) of opals and the role of "water" in these $SiO_2 \cdot nH_2O$ minerals. *Fortschritte der Mineralogie*, *52*(1), 17–51.

Lynne, B. Y., Campbell, K. A., Moore, J. N., & Browne, P. R. L. (2005). Diagenesis of 1900-year-old siliceous sinter (opal-A to quartz) at Opal Mound, Roosevelt Hot Springs, Utah, USA. *Sedimentary Geology*, *179*(3–4), 249–278. https://doi.org/10.1016/j.sedgeo.2005.05.012

Mahaffy, P. R., Webster, C. R., Cabane, M., Conrad, P. G., Coll, P., Atreya, S. K., et al. (2012). The Sample Analysis at Mars Investigation and Instrument Suite. *Space Science Reviews*, *170*(1–4), 401–478. https://doi.org/10.1007/s11214-012-9879-z

Marion, G. M., Catling, D. C., Kargel, J. S., & Crowley, J. K. (2016). Modeling calcium sulfate chemistries with applications to Mars. *Icarus*, *278*, 31–37. https://doi.org/10.1016/j.icarus.2016.05.016

Matheney, R. K., & Knauth, L. P. (1993). New isotopic temperature estimates for early silica diagenesis in bedded cherts. *Geology*, *21*(6), 519–522. https://doi.org/10.1130/0091-7613(1993)021<0519:NITEFE>2.3.CO;2

Maurice, S., Clegg, S. M., Wiens, R. C., Gasnault, O., Rapin, W., Forni, O., et al. (2016). ChemCam activities and discoveries during the nominal mission of the Mars Science Laboratory in Gale crater, Mars. *Journal of Analytical Atomic Spectrometry*, *31*(4), 863–889. https://doi.org/10.1039/C5JA00417A

Maurice, S., Wiens, R. C., Saccoccio, M., Barraclough, B., Gasnault, O., Forni, O., et al. (2012). The ChemCam Instrument Suite on the Mars Science Laboratory (MSL) Rover: Science objectives and mast unit description. *Space Science Reviews*, *170*(1–4), 95–166. https://doi.org/10.1007/s11214-012-9912-2

McCubbin, F. M., Smirnov, A., Nekvasil, H., Wang, J., Hauri, E., & Lindsley, D. H. (2010). Hydrous magmatism on Mars: A source of water for the surface and subsurface during the Amazonian. *Earth and Planetary Science Letters*, *292*(1-2), 132–138. https://doi.org/10.1016/j.epsl.2010.01.028

McLennan, S. M. (2003). Sedimentary silica on Mars. *Geology*, *31*(4), 315–318. https://doi.org/10.1130/0091-7613(2003)031<0315:SSOM>2.0.CO;2

Meister, P., Chapligin, B., Picard, A., Meyer, H., Fischer, C., Rettenwander, D., et al. (2014). Early diagenetic quartz formation at a deep iron oxidation front in the eastern equatorial Pacific—A modern analogue for banded iron/chert formations? *Geochimica et Cosmochimica Acta*, *137*, 188–207. https://doi.org/10.1016/j.gca.2014.03.035

Meslin, P.-Y., Gasnault, O., Forni, O., Schröder, S., Cousin, A., Berger, G., et al. (2013). Soil diversity and hydration as observed by ChemCam at Gale crater, Mars. *Science*, *341*(6153), 1238670. https://doi.org/10.1126/science.1238670

Metz, J. M., Grotzinger, J. P., Mohrig, D., Milliken, R., Prather, B., Pirmez, C., et al. (2009). Sublacustrine depositional fans in southwest Melas Chasma. *Journal of Geophysical Research*, *114*, E10002. https://doi.org/10.1029/2009JE003365

Milliken, R. E., Swayze, G. A., Arvidson, R. E., Bishop, J. L., Clark, R. N., Ehlmann, B. L., et al. (2008). Opaline silica in young deposits on Mars. *Geology*, *36*(11), 847–850. https://doi.org/10.1130/G24967A.1

Mitrofanov, I., Litvak, M., Varenikov, A., Barmakov, Y., Behar, A., Bobrovnitsky, Y., et al. (2012). Dynamic Albedo of Neutrons (DAN) experiment onboard NASA's Mars Science Laboratory. *Space Science Reviews*, *170*(1–4), 559–582. https://doi.org/10.1007/s11214-012-9924-y

Morris, R. V., Vaniman, D. T., Blake, D. F., Gellert, R., Chipera, S. J., Rampe, E. B., et al. (2016). Silicic volcanism on Mars evidenced by tridymite in high-SiO_2 sedimentary rock at Gale crater. *Proceedings of the National Academy of Sciences of the United States of America*, *113*(26), 7071–7076. https://doi.org/10.1073/pnas.1607098113

Murata, K. J., & Nakata, J. K. (1974). Cristobalitic stage in the diagenesis of diatomaceous shale. *Science*, *184*(4136), 567–568. https://doi.org/10.1126/science.184.4136.567

Muster, T. H., Prestidge, C. A., & Hayes, R. A. (2001). Water adsorption kinetics and contact angles of silica particles. *Colloids and Surfaces A: Physicochemical and Engineering Aspects*, *176*(2-3), 253–266. https://doi.org/10.1016/S0927-7757(00)00600-2

Nachon, M., Clegg, S. M., Mangold, N., Schröder, S., Kah, L. C., Dromart, G., et al. (2014). Calcium Sulfate Characterized by ChemCam/Curiosity at Gale crater, Mars. *LPI Contributions*, *1791*, 1334.

Nachon, M., Mangold, N., Forni, O., Kah, L. C., Cousin, A., Wiens, R. C., et al. (2017). Chemistry of diagenetic features analyzed by ChemCam at Pahrump Hills, Gale crater, Mars. *Icarus*, *281*, 121–136. https://doi.org/10.1016/j.icarus.2016.08.026

Newman, S., Stolper, E. M., & Epstein, S. (1986). Measurement of water in rhyolitic glasses; calibration of an infrared spectroscopic technique. *American Mineralogist*, *71*(11–12), 1527–1541.

Palucis, M. C., Dietrich, W. E., Hayes, A. G., Williams, R. M. E., Gupta, S., Mangold, N., et al. (2014). The origin and evolution of the Peace Vallis fan system that drains to the Curiosity landing area, Gale crater, Mars. *Journal of Geophysical Research: Planets*, *119*, 705–728. https://doi.org/10.1002/2013JE004583

Palucis, M. C., Dietrich, W. E., Williams, R. M. E., Hayes, A. G., Parker, T., Sumner, D. Y., et al. (2016). Sequence and relative timing of large lakes in Gale crater (Mars) after the formation of Mount Sharp. *Journal of Geophysical Research: Planets*, *121*, 472–496. https://doi.org/10.1002/2015JE004905

Rampe, E. B., Ming, D. W., Blake, D. F., Bristow, T. F., Chipera, S. J., Grotzinger, J. P., et al. (2017). Mineralogy of an ancient lacustrine mudstone succession from the Murray formation, Gale crater, Mars. *Earth and Planetary Science Letters*, *471*, 172–185. https://doi.org/10.1016/j.epsl.2017.04.021

Rapin, W. (2016). Hydratation de la surface de Mars à partir des données du rover Curiosity (PhD thesis). Université Toulouse 3 Paul Sabatier (UT3 Paul Sabatier). Retrieved from https://tel.archives-ouvertes.fr/tel-01462123/document

Rapin, W., Bousquet, B., Lasue, J., Meslin, P.-Y., Lacour, J.-L., Fabre, C., et al. (2017b). Roughness effects on the hydrogen signal in laser-induced breakdown spectroscopy. *Spectrochimica Acta Part B: Atomic Spectroscopy*, *137*(Supplement C), 13–22. https://doi.org/10.1016/j.sab.2017.09.003

Rapin, W., Meslin, P.-Y., Maurice, S., Vaniman, D., Nachon, M., Mangold, N., et al. (2016). Hydration state of calcium sulfates in Gale crater, Mars: Identification of bassanite veins. *Earth and Planetary Science Letters*, *452*, 197–205. https://doi.org/10.1016/j.epsl.2016.07.045

Rapin, W., Meslin, P.-Y., Maurice, S., Wiens, R. C., Laporte, D., Chauviré, B., et al. (2017a). Quantification of water content by laser induced breakdown spectroscopy on Mars. *Spectrochimica Acta Part B: Atomic Spectroscopy*, *130*, 82–100. https://doi.org/10.1016/j.sab.2017.02.007

Rey, P. F. (2013). Opalisation of the Great Artesian Basin (central Australia): An Australian story with a Martian twist. *Australian Journal of Earth Sciences*, *60*(3), 291–314. https://doi.org/10.1080/08120099.2013.784219

Rice, M. S., Cloutis, E. A., Bell, J. F. III, Bish, D. L., Horgan, B. H., Mertzman, S. A., et al. (2013). Reflectance spectra diversity of silica-rich materials: Sensitivity to environment and implications for detections on Mars. *Icarus*, *223*(1), 499–533. https://doi.org/10.1016/j.icarus.2012.09.021

Rickert, D., Schlüter, M., & Wallmann, K. (2002). Dissolution kinetics of biogenic silica from the water column to the sediments. *Geochimica et Cosmochimica Acta*, *66*(3), 439–455. https://doi.org/10.1016/S0016-7037(01)00757-8

Rodgers, K. A., Browne, P. R. L., Buddle, T. F., Cook, K. L., Greatrex, R. A., Hampton, W. A., et al. (2004). Silica phases in sinters and residues from geothermal fields of New Zealand. *Earth-Science Reviews*, *66*(1-2), 1–1), 61. https://doi.org/10.1016/j.earscirev.2003.10.001

Rondeau, B., Cenki-Tok, B., Fritsch, E., Mazzero, F., Gauthier, J.-P., Bodeur, Y., et al. (2012). Geochemical and petrological characterization of gem opals from Wegel Tena, Wollo, Ethiopia: Opal formation in an Oligocene soil. *Geochemistry: Exploration, Environment, Analysis*, *12*(2), 93–104. https://doi.org/10.1144/1467-7873/10-MINDEP-058

Ruff, S. W., Farmer, J. D., Calvin, W. M., Herkenhoff, K. E., Johnson, J. R., Morris, R. V., et al. (2011). Characteristics, distribution, origin, and significance of opaline silica observed by the Spirit rover in Gusev crater, Mars. *Journal of Geophysical Research*, *116*, E00F23. https://doi.org/10.1029/2010JE003767

Savijärvi, H., Harri, A.-M., & Kemppinen, O. (2016). The diurnal water cycle at Curiosity: Role of exchange with the regolith. *Icarus*, *265*, 63–69. https://doi.org/10.1016/j.icarus.2015.10.008

Schmidt, P., & Fröhlich, F. (2011). Temperature dependent crystallographic transformations in chalcedony, SiO2, assessed in mid infrared spectroscopy. *Spectrochimica Acta Part A: Molecular and Biomolecular Spectroscopy*, *78*(5), 1476–1481. https://doi.org/10.1016/j.saa.2011.01.036

Seelos, K. D., Seelos, F. P., Viviano-Beck, C. E., Murchie, S. L., Arvidson, R. E., Ehlmann, B. L., & Fraeman, A. A. (2014). Mineralogy of the MSL Curiosity landing site in Gale crater as observed by MRO/CRISM. *Geophysical Research Letters*, *41*, 4880–4887. https://doi.org/10.1002/2014GL060310

Segnit, E. R., Stevens, T. J., & Jones, J. B. (1965). The role of water in opal. *Journal of the Geological Society of Australia*, *12*(2), 211–226. https://doi.org/10.1080/00167616508728593

Sklute, E. C., Jensen, H. B., Rogers, A. D., & Reeder, R. J. (2015). Morphological, structural, and spectral characteristics of amorphous iron sulfates. *Journal of Geophysical Research: Planets*, *120*, 809–830. https://doi.org/10.1002/2014JE004784

Skok, J. R., Mustard, J. F., Ehlmann, B. L., Milliken, R. E., & Murchie, S. L. (2010). Silica deposits in the Nili Patera caldera on the Syrtis Major volcanic complex on Mars. *Nature Geoscience*, *3*(12), 838–841. https://doi.org/10.1038/ngeo990

Smith, M. R., Bandfield, J. L., Cloutis, E. A., & Rice, M. S. (2013). Hydrated silica on Mars: Combined analysis with near-infrared and thermal-infrared spectroscopy. *Icarus*, *223*(2), 633–648. https://doi.org/10.1016/j.icarus.2013.01.024

Stolper, E. (1982). Water in silicate glasses: An infrared spectroscopic study. *Contributions to Mineralogy and Petrology*, *81*(1), 1–17. https://doi.org/10.1007/BF00371154

Sun, V. (2017). *Clays and opals on Mars: Implications for water-rock interactions through time*. Providence, RI: Brown University. https://doi.org/10.7301/Z08G8J58

Sun, V. Z., & Milliken, R. E. (2015). Ancient and recent clay formation on Mars as revealed from a global survey of hydrous minerals in crater central peaks. *Journal of Geophysical Research: Planets*, *120*, 2293–2332. https://doi.org/10.1002/2015JE004918

Sutter, B., McAdam, A. C., Mahaffy, P. R., Ming, D. W., Edgett, K. S., Rampe, E. B., et al. (2017). Evolved gas analyses of sedimentary rocks and eolian sediment in Gale crater, Mars: Results of the Curiosity rover's Sample Analysis at Mars (SAM) instrument from Yellowknife Bay to the Namib Dune. *Journal of Geophysical Research: Planets*, *122*, 2574–2609. https://doi.org/10.1002/2016JE005225

Thiry, M., & Milnes, A. R. (1991). Pedogenic and groundwater silcretes at Stuart Creek Opal Field, South Australia. *Journal of Sedimentary Research*, *61*(1), 111–127.

Thiry, M., Milnes, A. R., Rayot, V., & Simon-CoinÇon, R. (2006). Interpretation of palaeoweathering features and successive silicifications in the Tertiary regolith of inland Australia. *Journal of the Geological Society*, *163*(4), 723–736. https://doi.org/10.1144/0014-764905-020

Thomas, P., Šimon, P., Smallwood, A., & Ray, A. (2007). Estimation of the diffusion coefficient of water evolved during the non-isothermal dehydration of Australian sedimentary opal. *Journal of Thermal Analysis and Calorimetry*, *88*(1), 231–235. https://doi.org/10.1007/s10973-006-8133-x

Thomas, P. S., Heide, K., & Földvari, M. (2015). Water and hydrogen release from perlites and opal. *Journal of Thermal Analysis and Calorimetry*, *120*(1), 95–101. https://doi.org/10.1007/s10973-014-4336-8

Thomas, P. S., Šesták, J., Heide, K., Fueglein, E., & Šimon, P. (2010). Thermal properties of Australian sedimentary opals and Czech moldavites. *Journal of Thermal Analysis and Calorimetry*, *99*(3), 861–867. https://doi.org/10.1007/s10973-010-0706-z

Thomson, B. J., Bridges, N. T., Milliken, R., Baldridge, A., Hook, S. J., Crowley, J. K., et al. (2011). Constraints on the origin and evolution of the layered mound in Gale crater, Mars using Mars Reconnaissance Orbiter data. *Icarus*, *214*(2), 413–432. https://doi.org/10.1016/j.icarus.2011.05.002

Tosca, N. J., & Knoll, A. H. (2009). Juvenile chemical sediments and the long term persistence of water at the surface of Mars. *Earth and Planetary Science Letters*, *286*(3–4), 379–386. https://doi.org/10.1016/j.epsl.2009.07.004

Vasavada, A. R., Piqueux, S., Lewis, K. W., Lemmon, M. T., & Smith, M. D. (2017). Thermophysical properties along Curiosity's traverse in Gale crater, Mars, derived from the REMS ground temperature sensor. *Icarus*, *284*, 372–386. https://doi.org/10.1016/j.icarus.2016.11.035

Wang, A., Freeman, J. J., & Jolliff, B. L. (2009). Phase transition pathways of the hydrates of magnesium sulfate in the temperature range 50°C to 5°C: Implication for sulfates on Mars. *Journal of Geophysical Research*, *114*, E04010. https://doi.org/10.1029/2008JE003266

Weitz, C. M., Milliken, R. E., Grant, J. A., McEwen, A. S., Williams, R. M. E., Bishop, J. L., & Thomson, B. J. (2010). Mars Reconnaissance Orbiter observations of light-toned layered deposits and associated fluvial landforms on the plateaus adjacent to Valles Marineris. *Icarus*, *205*(1), 73–102. https://doi.org/10.1016/j.icarus.2009.04.017

Wiens, R. C., Maurice, S., Barraclough, B., Saccoccio, M., Barkley, W. C., Iii, J. F. B., et al. (2012). The ChemCam Instrument Suite on the Mars Science Laboratory (MSL) rover: Body unit and combined system tests. *Space Science Reviews*, *170*(1–4), 167–227. https://doi.org/10.1007/s11214-012-9902-4

Wiens, R. C., Maurice, S., & Team, M. S. (2015). ChemCam: Chemostratigraphy by the first Mars microprobe. *Elements*, *11*(1), 33–38. https://doi.org/10.2113/gselements.11.1.33

Williams, L. A., & Crerar, D. A. (1985). Silica diagenesis; II, General mechanisms. *Journal of Sedimentary Research*, *55*(3), 312–321. https://doi.org/10.1306/212F86B1-2B24-11D7-8648000102C1865D

Williams, L. A., Parks, G. A., & Crerar, D. A. (1985). Silica diagenesis, I. Solubility Controls. *Journal of Sedimentary Research*, *55*(3), 301–311.

Wray, J. J., Milliken, R. E., Dundas, C. M., Swayze, G. A., Andrews-Hanna, J. C., Baldridge, A. M., et al. (2011). Columbus crater and other possible groundwater-fed paleolakes of Terra Sirenum, Mars. *Journal of Geophysical Research*, *116*, E01001. https://doi.org/10.1029/2010JE003694

Yen, A. S., Ming, D. W., Vaniman, D. T., Gellert, R., Blake, D. F., Morris, R. V., et al. (2017). Multiple stages of aqueous alteration along fractures in mudstone and sandstone strata in Gale crater, Mars. *Earth and Planetary Science Letters*, *471*, 186–198. https://doi.org/10.1016/j.epsl.2017.04.033

Zhang, Y. (1999). H2O in rhyolitic glasses and melts: Measurement, speciation, solubility, and diffusion. *Reviews of Geophysics*, *37*(4), 493–516. https://doi.org/10.1029/1999RG900012